

Supporting Information

Damage assessment from high-resolution images

The examination of TPLSM image stacks indicates that the majority of vessels in the neighborhood of the target (yellow circles in figures 8A and 8B) were structurally unaffected by the laser light. Most vessels near the clot do not show extravasation, an effect associated with vessel damage (1). Critically, fast and slow flow is observed in vessels close to the occluded target vessel (Fig. 8A1). Although flow is extremely slow in many vessels, the motion of RBCs indicates that vessels away from the target are not occluded. In particular, movement of RBCs could often be observed in the penetrating vessel below the clot (final panel in figure 8B3). While we could not verify that clots never formed in the penetrating arteriole below the first lateral branch, the vasculature outside the target range was, for the most part, patent. In two exceptional cases, as shown by the examples of figure 8, an unconnected vessel (circled in blue in figure 8A) and the first lateral vessel (circled in blue in figure 8B) that branches off the penetrating vessel (circled in yellow in figure 8) were clotted. These vessels show some extravasation of the fluorescein/dextran dye, an effect associated with vessel damage (1). A final exceptional case concerns vessels directly beneath the irradiated zone that do not appear to have leaked fluorescently labeled dye, yet contain RBCs that are completely stationary (Fig. 8B1). To avoid such potentially directly clotted vessels, we were careful not to measure blood flow in areas directly beneath the irradiated zone.

Analysis of spatial distribution of penetrating arterioles

The change in distance, Δr , to the nearest penetrating arteriole from before, $r_{baseline}$, and after, $r_{postclot}$, a clot to a penetrating arteriole was calculated (Fig. 9) for the penetrating arteriole locations measured from four animals. We manually identified and noted the locations of each penetrating arteriole. The distance between each pixel in the image and the nearest diving arteriole was calculated numerically to form the distribution of $r_{baseline}$. To simulate the effect of clotting a penetrating arteriole, we deleted each penetrating arteriole one at a time in simulations and recalculated the distance from each pixel to the nearest penetrating arteriole, to form the distribution $r_{postclot}$. Further, for each pixel we calculated the difference $\Delta r \equiv r_{postclot} - r_{baseline}$, which allowed us to define pairs of Δr and $r_{baseline}$. Note that calculations were carried out only on arteriolar territories that did not meet the edge of the imaging field so as to avoid over-counting.

The results of the above calculation were binned in 1- μm intervals of $r_{baseline}$, which is three-times over sampling, and Δr was averaged for each bin. The resultant plot of Δr versus $r_{baseline}$ for the measured penetrating arteriole locations is shown in figure 6C (thick solid red).

We used the above algorithm to calculate Δr as a function of $r_{baseline}$ for vessels arranged in three regular lattices: a triangular lattice, a square, and a hexagonal lattice. We used the mean nearest neighboring arteriole distance measured from the image data as the nearest-neighboring distance in the regular lattices and used the same-size field, 2.3 mm x 2.3 mm, and pixel size, 3 μm x 3 μm , as the TPLSM images. The results are plotted as thin dotted lines in Figure 6C, which appear very different than the data. Lastly, we calculated Δr as a function of $r_{baseline}$ for a randomly arranged lattice in which the mean number of penetrating arterioles per area was equal to the experimentally measured value of 13 vessels per mm^2 . The curve from an example of a randomly generated lattice is also shown in figure 6C (dotted black line).

We also found an analytical expression for the dependence of Δr on $r_{baseline}$ at any point x and y , where $(x, y) = (0,0)$ is the location of the clotted arteriole and (x_n, y_n) describes the location of all the other penetrating arterioles. In regular lattices, symmetry may be used to calculate Δr in a small area in which (x_0, y_0) describes the location of the next-nearest-penetrating arteriole at $(x_0, y_0) = (a, 0)$, where a is the distance between nearest-neighboring penetrating arterioles; experimentally, $a = 130 \mu\text{m}$. We note that

$$\Delta r(x, y) = \sqrt{(x - x_0)^2 + (y - y_0)^2}.$$

This expression may be expressed the polar coordinates θ and $r_{baseline}$. For brevity we abbreviate $r_{baseline}$ as r_b . We find

$$\Delta r(r_b, \theta) = \sqrt{r_b^2 + a^2 - 2ar_b \cos \theta}.$$

The above expression is averaged over angles, θ , to form the dependence of Δr on r_b . The integral can be divided into two regions:

$$\Delta r(r_b) = \frac{1}{\theta_{\max}} \int_0^{\theta_{\max}} d\theta \sqrt{r_b^2 + a^2 - 2ar_b \cos \theta} \quad \text{for } r_b < \frac{a}{2}$$

$$= \frac{1}{\theta_{\max} - \cos^{-1}\left(\frac{a}{2r_b}\right)} \int_{\cos^{-1}\left(\frac{a}{2r_b}\right)}^{\theta_{\max}} d\theta \sqrt{r_b^2 + a^2 - 2ar_b \cos \theta} \quad \text{for } \frac{a}{2} \leq r_b \leq \frac{a}{2 \cos \theta_{\max}}$$

where $\theta_{\max}=\pi/4$ for a square lattice, $\theta_{\max}=\pi/6$ for a triangular lattice and $\theta_{\max}=\pi/3$ for a hexagonal lattice (Fig. 10). These integrals were evaluated numerically and the results are plotted as thin, solid lines in figure 6C.

MODEL OF BLOOD FLOW CHANGES AFTER PENETRATING ARTERIOLE OCCLUSION

We developed a geometric model that relates the spatial distribution of penetrating arterioles (Figs. 6A to 6C) to the decrement in blood flow that occurs upon occlusion of penetrating arteriole (Figs. 3A and 3B). We assume the average volume flux through a penetrating arteriole is $F = 2/3\pi b^2 v$, where b is the radius of the arteriole, and v is the mean speed of RBCs through the arteriole. The return path of this blood is ultimately through venules that emerge through the cortical surface. The volume flux of RBC that enters the cortex through a penetrating arteriole must equal the spatially integrated flux of venous blood that exits the tissue. We denote the spatial distribution of the exiting flux as $f(r, \phi) dA$, where f is a function that represents the speed of blood that exits the region of cortex that is centered around a penetrating vessel at the origin and $dA = r d\phi dr = dx dy$ is an element of area.

For simplicity of calculation, we assume that the spatial distribution of the blood that exits the surface can be approximated as a smooth function that is cylindrically symmetric. We further assume that all penetrating vessels have the same average flux, F , and same radius b . Conservation of RBCs flowing in and out of the brain tissue leads to

$$\pi b^2 \langle v \rangle = \int_{-\pi}^{\pi} d\phi \int_b^{\infty} r dr f(r) = 2\pi \int_b^{\infty} r dr f(r).$$

The function $f(r)$ can have any form that allows the above integral to have a finite value. For example, a Gaussian function for the flow, *i.e.*,

$$f(r) = k e^{-\frac{r^2}{2\sigma^2}}.$$

where k is a normalization constant, satisfies these criteria, as does an exponential decay, *i.e.*,

$$f(r) = k e^{-r/\lambda}.$$

We consider an additional model for the distribution of blood from penetrating arterioles as a means to access the territory affected by the blockage of one penetrating arteriole. We take a tree-like branching pattern for the capillary network (Fig. 11A), in which all capillaries have the same cross-sectional area, denoted a , and have straight segments between branches of length λ . This pattern ignores collaterals, the tortuous nature of capillaries, the anisotropy in the distributions of vessels, and the draining of blood flow via a network of venules that return to the surface. Yet, as the statistics of microvessel networks are yet unmeasured, the model provides a starting point for an estimate of the scaling of blood speed.

The total capillary area, A_{Total} , as a function of the distance, r , from the origin of the primary branch of the capillary tree at the arteriole scales as:

$$A_{\text{Total}} = N \cdot a \cdot 2^{r/\lambda}$$

where N is the number of primary branches that emanate from the arteriole.

We let F denote the flux of blood into the penetrating arteriole, *i.e.*, the volume of blood per unit time. The total flux out of the cortical region fed by a given penetrating arteriole must equal the flux in, by conservation of mass. We assume that the speed as a function of distance can be describe as a continuous function, denoted $f(r)$. Therefore, the product of the area and the speed must be constant and equal to the incoming flux, *i.e.*,

$$F = f(r) \cdot A_{\text{Total}} = f(r) \cdot N \cdot a \cdot 2^{r/\lambda}$$

Solving for $f(r)$ yields

$$f(r) = \frac{F}{N \cdot a} e^{-r/\lambda},$$

where $\lambda' = \lambda/\ln 2$. This suggests that the functional form of the contribution of blood flow speeds around a penetrating arteriole is exponentially decaying.

We next assume that at a given location of cortex, labeled by (x, y) , the speed of blood flow is proportional to the sum over all penetrating arterioles

$$S_{\text{Total}}(x, y) = \sum_{n=1}^N f(x - x_n, y - y_n)$$

where $x = r \cos\phi$, $y = r \sin\phi$, n labels the penetrating arterioles, and N is the number of penetrating arterioles. To model the percentage of baseline speed after the occlusion of one penetrating vessel, we calculate the ratio of $S_{\text{Total}}(x, y)$ with one vessel excluded to $S_{\text{Total}}(x, y)$ with all vessels unperturbed, *i.e.*,

$$\text{Fraction of baseline speed (r)} = \frac{\sum_{\substack{n=1 \\ n \neq m}}^N f(x - x_n, y - y_n)}{\sum_{n=1}^N f(x - x_n, y - y_n)}$$

where m labels the blocked penetrating arteriole. Note that the constant factor k cancels out. The above fraction can be compared with the data, *cf* figures 10B and 3B. The calculated fraction was calculated for exponentially decaying function $e^{-r/\lambda'}$ for blood flow with several values of the constant λ' . Average capillary lengths are $\sim 50 \mu\text{m}$ between two branch points (2). Curvature in a semicircle, as a rough estimate of tortuosity, yields $\lambda' = 40 \mu\text{m}$.

REFERENCES

1. Schaffer, CB, Friedman, B, Nishimura, N, Schroeder, LF, Tsai, PS, Ebner, FF, Lyden, PD and Kleinfeld, D (2006) Two-photon imaging of cortical surface microvessels reveals a robust redistribution in blood flow after vascular occlusion. *Public Library of Science, Biology* **4**,258-270.
2. Tata, DA and Anderson, BJ (2002) A new method for the investigation of capillary structure. *J. Neurosci. Methods* **113**,199-206.

Supporting Information – Figure Legends

Figure 8. Blood flow in vessels in the immediate neighborhood of the clot. Two independent examples are shown. **(A)** Side projection in the coronal plane of TPLSM image stacks around a penetrating arteriole clots. Yellow ellipse indicates the location of the penetrating clots. Blue ellipse indicates a vessel just below the target vessel that was found to be clotted and further shows extravasation. **(A1 through A3)** Projections in the tangential plane through the radial ranges indicated in part A. The green arrows from specific vessel segments (red) point to images and line-scans taken both before and after the induction of clots in the penetrating arteriole. Note that while RBC flow was mostly reduced, the speed in one vessel close to the clot actually increased (A1). Panels A1 and A2 are used to construct figure 4 in the main text. **(B)** Second example, notation as in panel A. **(B1 and B3)** Projections in the tangential plane, similar to those panels A1 through A3. Note that one vessel stalled after the clot and no line-scan is shown for the stall (B1). All scale bars in images of individual vessels are 10 μm .

Figure 9. Penetrating arteriole territories. (A and B) The distance from each pixel to its nearest penetrating arteriole before (panel A) and after (panel B) the removal of a penetrating arteriole. These images show calculated distances in a central region. The black line outlines the territory of the removed arteriole. The grey shading indicates arteriole territories that extended to the edge of the image and were therefore excluded from our analysis.

Figure 10. Regular lattices for calculation of Δr with regions of integration. The red dots indicate the locations of penetrating arterioles. The blue shading indicates the region in which $r_{baseline} < \frac{a}{2}$ and the red shading shows region in which $\frac{a}{2} \leq r_{baseline} \leq \frac{a}{2 \cos \theta_{max}}$. In all three lattices, the nearest-neighbor distance between arterioles, a , is equal to 130 μm .

Figure 11. Model of blood flow versus distance from a penetrating arteriole. (A) A schematic of a model of branching blood vessels in which the cross-sectional area is a , and the distance between branch points measured radially is λ . **(B)** Calculated fraction of baseline flow after occlusion of penetrating arteriole as modeled by exponentially decaying functions modeling

the contribution to blood flow from a penetrating arteriole. Average of data and SEM from figure 3B is reproduced here in black and gray lines.

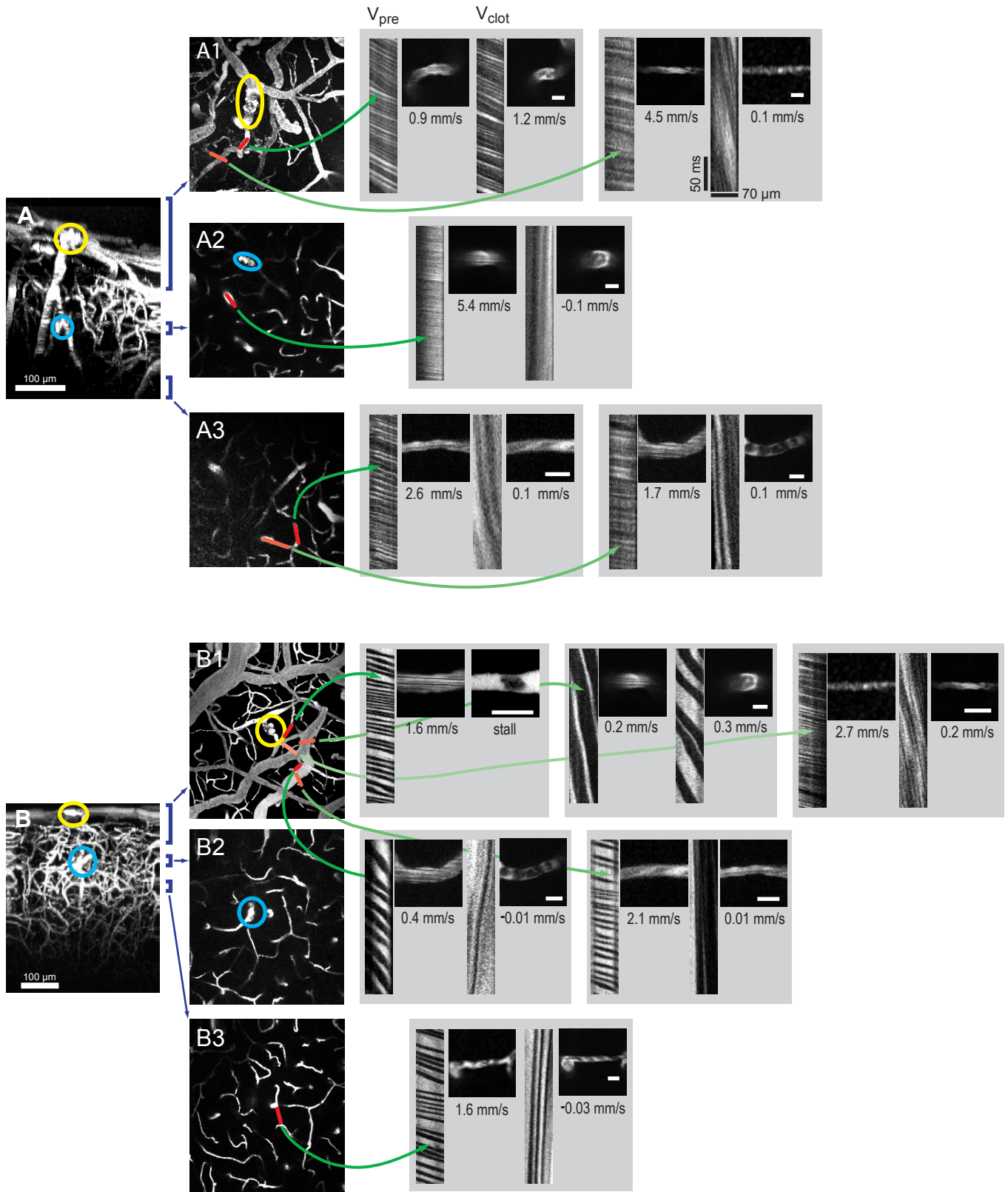


Figure 8 - Supplementary Information - Nishimura, Schaffer, Friedman, Lyden and Kleinfeld

Distance to nearest diving vessel (μm)

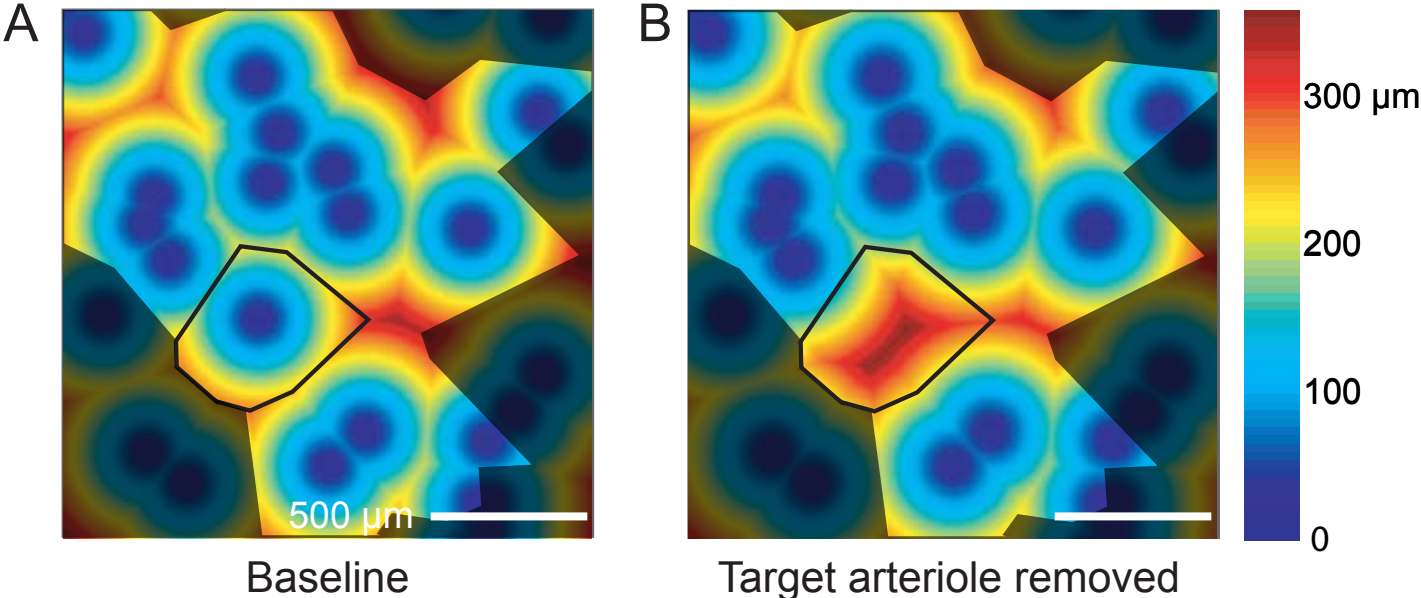


Figure 9 - Supplementary Information - Nishimura, Schaffer, Friedman, Lyden and Kleinfeld

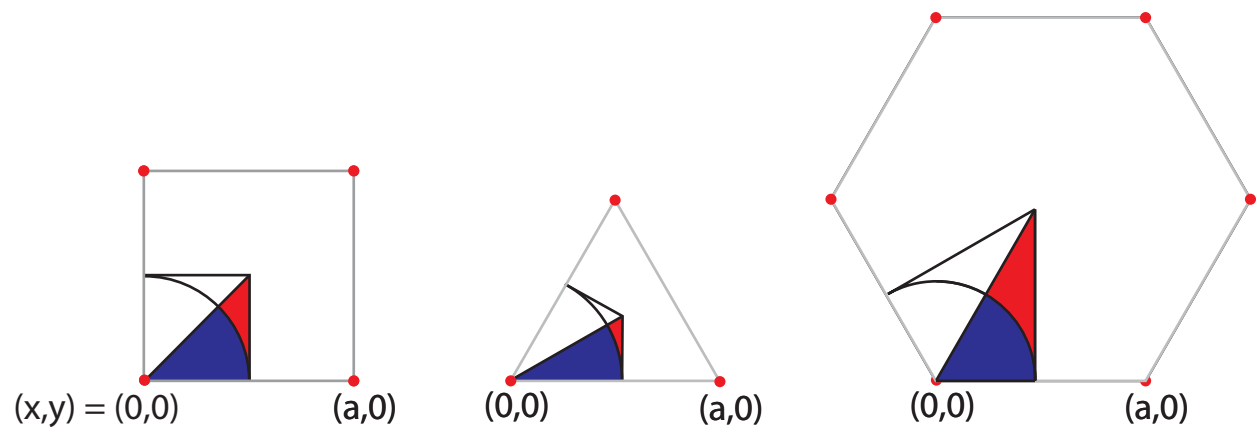


Figure 10 - Supplementary Information - Nishimura, Schaffer, Friedman, Lyden and Kleinfeld

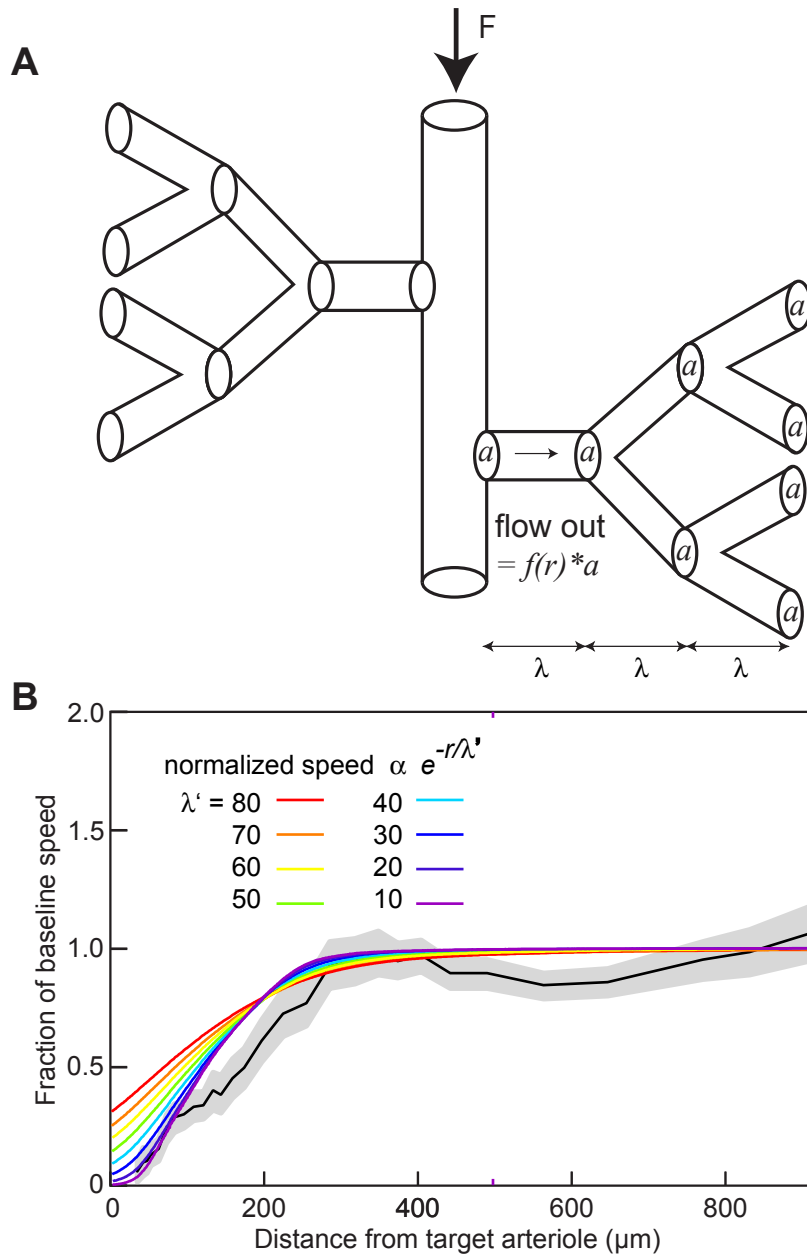


Figure 11 - Supplementary Information - Nishimura, Schaffer, Friedman, Lyden and Kleinfeld